第 48 卷 第 2 期/2021 年 1 月/中国激光 研究论文

中国激光

双光子聚合制备聚苯胺微结构

王荣荣[1,3]，张维彩[1,3]，金峰[1]，董贤子[1]，刘洁[1]，曲良体[2]，郑美玲[1*]

[1]中国科学院理化技术研究所仿生智能界面科学中心，北京 100190；

[2]清华大学机械与工程学院，北京 100084；

[3]中国科学院大学未来技术学院，北京 101407

摘要 为直接制备小尺度且具有可控形貌的导电聚合物微结构，利用一种基于飞秒激光的双光子聚合法，实现了聚苯胺在基底上任意位置处微纳米尺寸线条的精准可控制备。以苯胺为单体、硝酸为氧化剂，通过调控苯胺与硝酸的浓度，可以制备出具有不同形貌的聚苯胺微纳米线。不溶于水的苯胺高聚物在水相界面处合成，苯胺与硝酸的浓度及激光功率会影响水溶性苯胺低聚物的分布，进而影响聚苯胺微纳米线的形貌。当苯胺与硝酸浓度分别为 0.69 mol·L^{-1} 和 0.60 mol·L^{-1} 时，可制备出具有致密光滑形态、电导率为 5.79×10^{-6} S·cm^{-1} 的聚苯胺微纳米线。本研究为导电聚合物的制备及其在传感器、微型探测器等微纳米器件中的广泛应用提供了新思路。

关键词 激光光学；微纳结构；双光子聚合；导电聚合物；聚苯胺

中图分类号 O621.3 **文献标志码** A **doi**：10.3788/CJL202148.0202006

1 引 言

聚苯胺(R)作为一种重要的导电高分子材料，因其原料成本低、环境稳定性好、掺杂特性好等优势[1-2]，在能源储存[3-4]、化学检测[5]、生物传感器[6]和防腐涂料[7]等多种领域有着广阔的应用前景。聚苯胺的微观结构形貌是影响其性能的重要因素[8]，形貌规整的微纳米结构可提供离子与电荷的高速传输通道，这对其电化学性能的提高至关重要。目前制备聚苯胺微纳米结构的方法主要有溶液聚合法[1]、模板法、自组装法[9]、电化学法[10-11]等，这些方法制备的聚苯胺微结构多为一维或二维的大面积纳米纤维膜阵列，虽然在纤维膜阵列中的单根聚苯胺线宽度可小于 100 nm，但在大尺度阵列下纳米结构的均一性、制备灵活性差，生长不易控制，因此无法获得精准可控的聚苯胺微纳米结构，这对器件的集成化、微型化不利。

双光子聚合是基于材料的双光子吸收效应的光聚合方法。飞秒激光的超短脉宽、超高精度以及低热输入等特点[12-15]，可以控制光聚合材料在微纳尺度的定点区域内发生双光子聚合反应，进而实现任意复杂三维微纳米结构的制备。目前的双光子聚合材料多为商用光刻胶[16-18]、水凝胶[19-21]等，比如 Kawata 等[16]使用 SCR500 光刻胶制备了高精度三维“纳米牛”，Gou 等[19]利用聚乙二醇水凝胶制备了不同大小、形态的“红细胞”。这些双光子聚合材料可用于三维加工，具有较好的生物相容性，但其聚合物不具有导电性。苯胺可在光激发下发生光致聚合[22-23]，从而有望实现导电聚苯胺的制备。

本文提出利用飞秒激光双光子聚合制备尺寸、形貌可控的聚苯胺微纳米线的方法。该方法以苯胺为单体、硝酸为氧化剂，通过调控两者之间的浓度比、激光功率和扫描速度等参数，制备了不同形貌的聚苯胺微纳米线。聚苯胺微纳结构的精准可控制备有望为导电聚合物在集成化器件中的发展提供一种新方案。

2 实验部分

2.1 实验过程

苯胺混合溶液的制备(图 1)：将苯胺(Aniline)、

收稿日期：2020-08-31；**修回日期**：2020-10-13；**录用日期**：2020-10-28

基金项目：国家重点研发计划(2017YFB1104300)、国家自然科学基金(61975213，61475164，91323301)

*E-mail：zhengmeiling@mail.ipc.ac.cn

超纯水和硝酸(Nitric Acid)按照一定物质的量比依次加到 3 mL 溶剂瓶中,摇晃均匀,得到一系列总体积为 1000 μL 的苯胺混合溶液,此过程需在避光条件下进行。

苯胺混合溶液在基底上的固定:取一片洁净的玻璃片作为基底,中间放置一次性回形垫片,用 100 μL 移液枪取一滴苯胺混合溶液并将其转移至回形垫片中央,然后轻轻附上另一片洁净玻璃片,使苯胺溶液在垫片的回形空间内充分铺展,直至固定不流动,以此确保苯胺混合溶液在衬底表面上均匀分布。

苯胺混合溶液的双光子聚合:将制作好的苯胺混合溶液基底放置在飞秒激光双光子聚合系统的三维移动台上,进行双光子聚合。

聚苯胺的显影及干燥:首先用镊子轻轻去掉上层玻璃片和回形垫片,然后利用去离子水冲洗掉残留的苯胺混合溶液,经干燥后得到的聚苯胺微结构附着在基底玻璃片上。

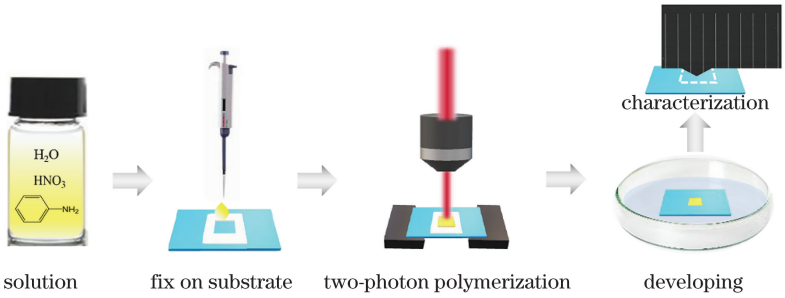

图 1 聚苯胺微结构制作工艺示意图

Fig. 1 Schematic diagram of polyaniline microstructure fabrication process

2.2 飞秒激光双光子聚合系统

本实验采用钛蓝宝石激光器(Tsunami, Spectra-Physics)作为激发光源,其中激光器的输出波长为 780 nm,重复频率为 80 MHz,脉冲宽度为 100 fs。如图 2 所示,飞秒激光经过一系列的光学器件,实现了激光光强的均匀分布以及激光的扩束,激光再通过油浸式高数值孔径(NA = 1.42, ×60)的物镜,最后聚焦到苯胺混合溶液中。计算机可通过控制光路中的快门、衰减器和移动台来调控聚苯胺微结构的制备过程,主要通过改变扫描速度和激光功率实现对结构精细度的控制。同时,聚苯胺的制

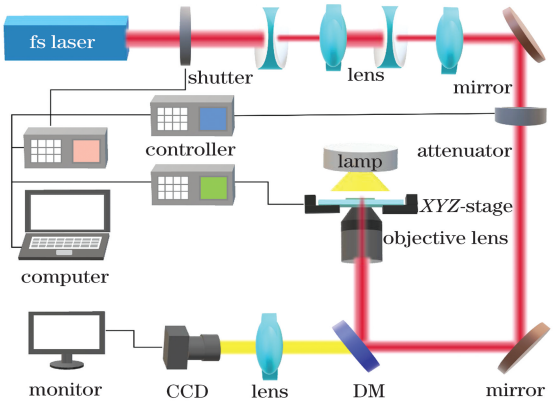

图 2 飞秒激光双光子聚合系统示意图

Fig. 2 Schematic diagram of femtosecond laser two-photon polymerization system

2.3 性能测试

使用扫描电子显微镜(SEM, S-4800, Hitachi, 日本)观察聚苯胺微结构的形貌特征。运用原子力显微镜(AFM, Icon2-sys, Bruker Nano Inc.,美国)观察聚苯胺微纳米线的横截面轮廓并计算其横截面面积。采用傅里叶变换红外光谱仪(FT-IR, Vertex 70v, Bruker, 德国)对硅基底上的聚苯胺样品进行 FT-IR 光谱测试。利用微操作低温探针台-半导体特征参数分析仪(CRX-4K, 4200-SCS)在氮气气氛下测定单根聚苯胺纳米线的电流-电压(C-V)曲线及其电阻值。在测量电阻之前,使用 50 目铜网覆盖在基底上的单根聚苯胺微纳米线上,然后在其表面喷金 60 s,未被铜网覆盖的纳米线两端沉积的金层用作测试电极。

3 分析与讨论

3.1 苯胺混合溶液对聚苯胺微结构的影响

以往的研究表明,苯胺低聚物(R^*)溶于水,高聚物不溶于水,高聚物的合成主要发生在水相界面处[24],且苯胺单体与酸的物质的量比需控制在一个较小的范围内[25]。本实验首先配制了苯胺浓度依次增大、苯胺与硝酸的物质的量比在 1.1 附近的苯胺混合溶液(表 1),并利用双光子聚合进行聚苯胺纳米线的制备。图 3 是样品 1,2,3,4 所制得的聚苯

胺纳米线的 SEM 图像。实验发现，随着苯胺单体浓度的增大，利用双光子聚合制备的聚苯胺纳米线的形貌也发生了变化。如图 3(a)所示，采用样品 1(苯胺浓度为 0.53 mol·L^{-1})得到的聚苯胺纳米线线型良好，但线条比较薄，且不致密，表面布满裂纹。当苯胺单体浓度增大到 0.6 mol·L^{-1}(样品 2)，如图 3(b)所示，聚合获得的纳米线是由一个个均匀的凸包联结而成，凸包边缘有密集的刺状延伸。与样品 1 相比，线条更为致密厚实。继续增大苯胺浓度到 0.7 mol·L^{-1}(样品 3)，如图 3(c)所示，线条的凸包形貌明显弱于样品 2，整体趋于平缓，且相比于前两个样品，样品 3 的线条更加致密厚实。当苯胺浓度为 0.8 mol·L^{-1}(样品 4)时，从图 3(d)可看出，凸包形状已基本消失，且线条的宽度均一，但其表面仍有些许裂纹。因此，随着苯胺混合溶液浓度的变化，双光子聚合而成的聚苯胺纳米线表现为不同的形貌结构，不同的形貌与聚苯胺纳米线是否由凸包联结而成有关。在相同的激光功率和扫描速度下，当苯胺与硝酸的浓度比较小时(样品 1 和样品 4)，更易得到较为平直的聚苯胺纳米线。随着苯胺单体浓度的增加，聚苯胺纳米线条更为致密厚实。

表 1 苯胺混合溶液的浓度及其聚合参数

Table 1 Concentration of aniline mixed solution and polymerization parameters

Sample	Concentration of aniline /(mol·L^{-1})	Concentration of nitric acid /(mol·L^{-1})	Concentration ratio of aniline to nitric acid	Power /mW	Velocity /(μm·s^{-1})
1	0.53	0.5	1.05∶1	8.5	6
2	0.60	0.5	1.20∶1	9.0–10.0	10
3	0.70	0.6	1.17∶1	10.3	6
4	0.80	0.7	1.14∶1	7.3–8.1	10
5	0.69	0.6	1.14∶1	14.1	6
6	0.91	0.8	1.14∶1	8.5	6

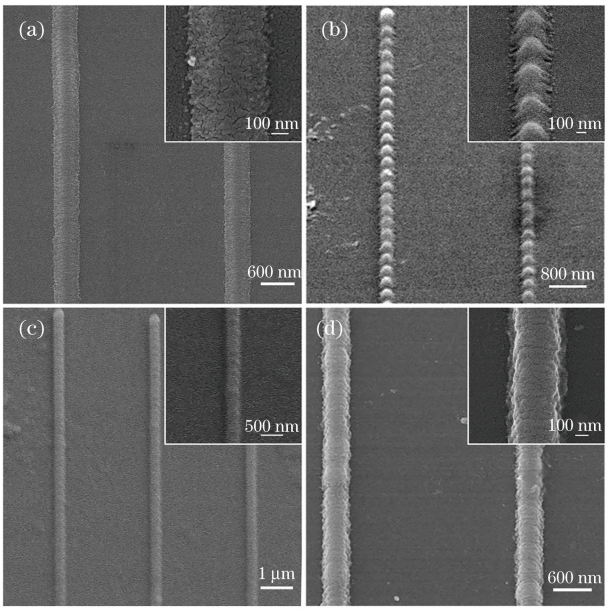

图 3 不同苯胺浓度的聚苯胺线的 SEM 图像。(a)样品 1；(b)样品 2；(c)样品 3；(d)样品 4

Fig. 3 SEM images of polyaniline lines with different aniline concentration. (a) Sample 1; (b) sample 2; (c) sample 3; (d) sample 4

图 4 是苯胺聚合机理示意图，激光以一定速度逐点扫描苯胺混合溶液时，在焦点处的硝酸根离子(NO_3^-)吸收光子形成氧阴离子自由基，氧阴离子自由基与水结合形成羟基自由基，羟基自由基攻击苯胺单体形成苯胺阳离子自由基，苯胺阳离子自由基原位结合形成苯胺低聚物。因苯胺低聚物可溶于水，而高聚物不溶于水，苯胺低聚物会迁移到水相界面处合成高聚物。飞秒激光的能量在空间上呈高斯分布，其光斑中心位置处的能量最高，激光能量从光斑中心向外逐渐降低[26]。将激光焦点调节在紧贴玻璃界面处，由于激光扫描方式为逐点扫描，扫描路径上的光强分布如图 4 所示，当苯胺浓度较低时(样品 1)，激光扫描路径上所有的苯胺单体都能在激光焦点处形成苯胺低聚物，这些低聚物在水相界面上聚合成薄薄的一层。但当苯胺浓度增大后，在相同的激光功率和扫描速度下，苯胺低聚物的形成区域与光能量的三维分布相对应，低聚物最先在玻璃基底水相界面处聚合成高聚物，远离界面的苯胺低聚物会向界面迁移，聚合过程中低聚物迁移去向与其迁移路径长短和迁移速度有关，低聚物会优先向距离相对较短(垂直)的成核位点聚集，从而形成如图 3(b)所示的凸包。当浓度继续增大(样品 3)，则相同高斯体积内低聚物浓度也增大，这些低聚物向凹陷

处扩散，使得凹陷更小。继续增大浓度，当苯胺单体浓度增加到一定值时（样品 4），线条的形貌会再次变得平整，并伴随着厚度增加。总之，因在激光焦点处苯胺单体与 NO_3^- 的浓度不同，苯胺阳离子自由基与苯胺低聚物的聚合位点不同，聚苯胺纳米线的形貌表现不同。

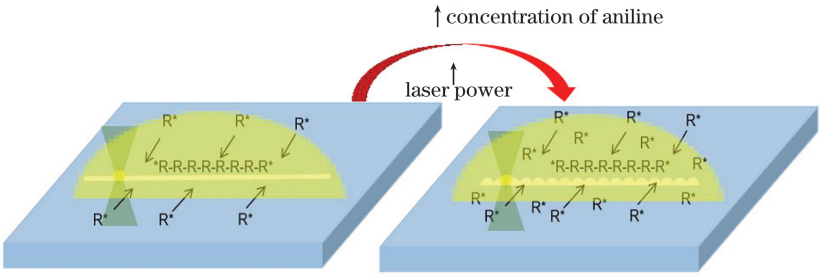

图 4　苯胺聚合机理示意图

Fig. 4　Schematic diagram of polymerization mechanism of aniline

尽管利用样品 1、2、3 和 4 都能制备出纳米线条，但受环境、移动台稳定性等的影响，重复加工时偶尔出现线条不连续的现象。为寻找导电性能和重复性能更好的聚苯胺，进一步优化了苯胺混合溶液，基于样品 4 的相对浓度为 1.14，分别降低或提高苯胺和硝酸的浓度，配制了样品 5 和样品 6，并考察了样品 5、6 的双光子聚合性能。图 5 是样品 5、6 合成的聚苯胺线的 SEM 图像。从图 5(a)中可以看出，激光功率和扫描速度基本相同时，降低浓度的样品 5 表现出较好的线条形貌和更好的加工性能，线条光滑，表面的裂纹消失，可一次性重复加工多条线。而对于样品 6，由于苯胺单体和 NO_3^- 浓度都比较大，激光扫过时瞬间产生大量自由基，爆聚现象严重，如图 5(b)所示。

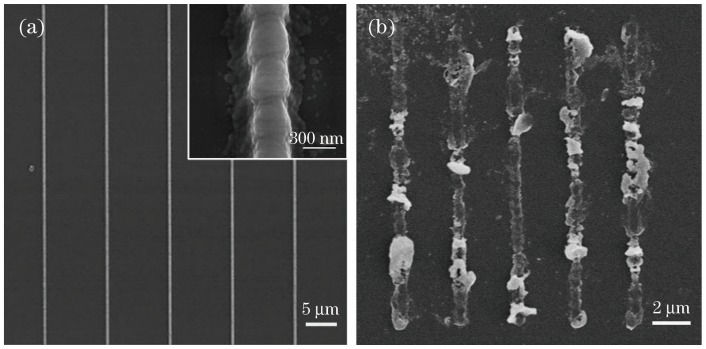

图 5　相对浓度为 1.14 时聚苯胺线的 SEM 图像。(a)样品 5；(b)样品 6

Fig. 5　SEM images of polyaniline lines at relative concentration of 1.14. (a) Sample 5; (b) sample 6

3.2　激光功率对聚苯胺微结构的影响

图 6 是样品 3 在扫描速度为 6 μm·s^{-1}、激光功率为 29 mW 的条件下聚合得到的结果，与图 3(c)中的样品 3 相比，图 6 中的凸包外形光滑，分布更加离散，在凸包底面还有一层很薄的线型沉积层，且该线型沉积层比其他样品在 10 mW 左右所得的线条宽一倍。这是因为加大激光功率后，激光的三维高斯分布直径相应地变高变宽，在这种情况下高斯峰顶处的苯胺低聚物的迁移路径更长，而且呈三维高斯分布的苯胺低聚物浓度和总量也都相应增大，这导致尽管扫描速度没有变化，但是峰顶低聚物来不及迁移到沉积薄层面聚合就结束了，这使得凸包的厚度增加，线条呈现出底层是沉积薄层、上面是凸包间隔分布的形态。

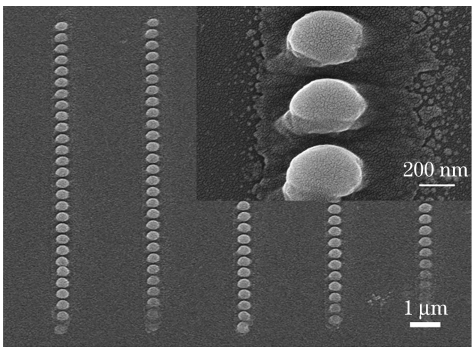

图 6　在 29 mW 功率下样品 3 制备的聚苯胺的 SEM 图像

Fig. 6　SEM image of polyaniline prepared by using sample 3 at laser power of 29 mW

3.3 扫描速度对聚苯胺微结构的影响

图 7(a)是样品 5 在 14.2 mW 的激光功率、1 ～ 10 μm·s^{-1} 的扫描速度下聚合得到的结果，图 7(b)是聚苯胺线的平均线宽与扫描速度的关系，其中平均线宽是对图 7(a)中的图像进行多次测量得到的平均值。如图 7 所示，激光扫描速度为 1 μm·s^{-1} 时，苯胺发生爆聚现象，之后随着扫描速度的增大，线条形貌变得规则可控，聚苯胺线条的分辨率也有所提高。而在激光扫描速度大于 7 μm·s^{-1} 时，随着扫描速度的进一步增大，线条宽度有所减小，且聚苯胺线条的形貌开始逐渐变得疏松。这是因为随着激光扫描速度的增加，焦点处曝光时间相应地减少，在光斑处引发的苯胺阳离子自由基减少，区域内形成的聚苯胺减少，从而导致线条更为疏松。反之，扫描速度过慢，对应的曝光时间过长，则会产生过多的自由基，这些自由基在苯胺溶液中急剧扩散从而引发内爆。因此，双光子聚合制备聚苯胺微结构需要在一定的激光扫描速度和曝光时间范围内进行。

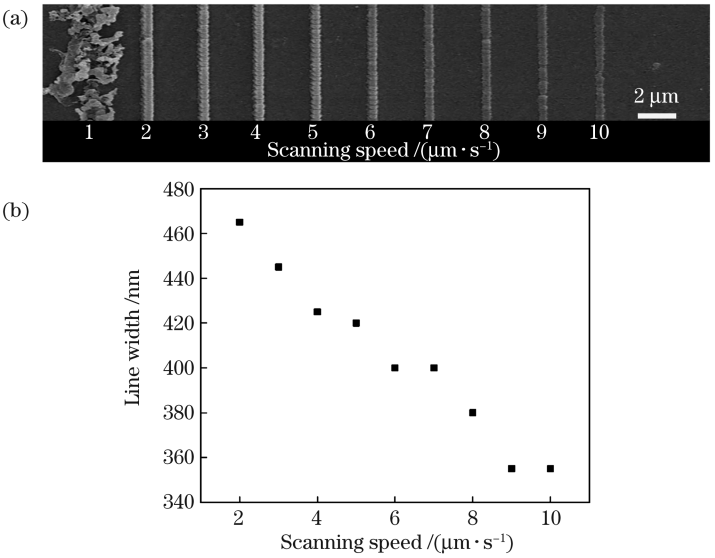

图 7 扫描速度对聚苯胺线条的影响。(a)扫描速度为 1～10 μm·s^{-1} 时聚苯胺线的 SEM 图像；(b)聚苯胺线的平均线宽与扫描速度的关系图

Fig. 7 Effect of scanning speed on polyaniline lines. (a) SEM image of polyaniline lines at scanning speed from 1 to 10 μm·s^{-1}; (b) relationship between scanning speed and average line width of polyaniline lines

3.4 聚苯胺微结构的红外光谱

利用双光子聚合法制备的微结构非常精细，利用傅里叶变换红外(FT-IR)光谱仪对精细结构进行了 FT-IR 测试，以验证其物质成分。图 8 是利用双光子聚合法制备的聚苯胺的 FT-IR 谱图。1597 cm^{-1} 和 1499 cm^{-1} 附近出现的较强特征峰，分别归属于苯环醌式结构(N＝Q＝N)和苯式结构(N-B-N)的 C＝C 伸缩振动，1698 cm^{-1} 处的特征峰归属为醌环结构的 C＝N 伸缩振动，1471 cm^{-1} 与 1444 cm^{-1} 处的峰则分别对应于醌环与苯环的骨架振动，而 1290 cm^{-1} 与 1208 cm^{-1} 处的特征峰分别为芳香胺 C－N、C＝N 的伸缩振动，1150 cm^{-1}、1108 cm^{-1} 附近的特征峰则分别归属于醌环和苯环上 C－H 的面内弯曲振动[27-28]。采用双光子聚合法得到的聚苯胺相较于其他文献中掺杂态的聚苯胺，特征吸收峰的位置向波数增大的方向发生了移动，这使得醌式结构和苯式结构中的电子云密度较高。

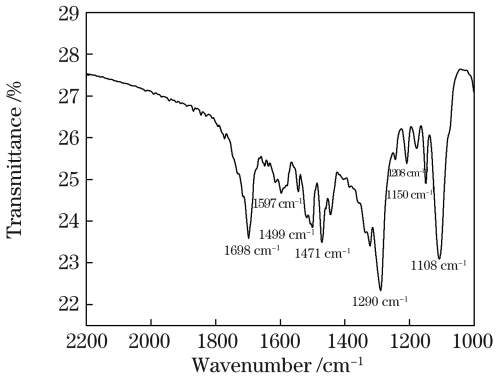

图 8 双光子聚合的聚苯胺微结构的 FT-IR 光谱

Fig. 8 FT-IR spectrum of two-photon polymerized polyaniline microstructure

3.5 聚苯胺微结构的导电性能

电导率是衡量导电聚合物导电性的指标，是材料传递电流能力的量度。一般认为，电导率小于 10^{-8} S·cm^{-1} 的材料为绝缘体，电导率大于

10^{-3} S·cm^{-1} 的材料为导体，而电导率在两者之间的材料为半导体。聚苯胺微结构的电导率可表示为

$$\sigma=\frac{L}{RS},\tag{1}$$

式中：σ 是电导率；L 是两电极间的距离；R 是样品电阻；S 是聚苯胺纳米线的横截面积。

本实验在样品 5 的条件下制备出一根 150 μm 长的聚苯胺纳米线，之后在其两端镀上一层金电极，两个电极间的距离 L 为 80 μm。利用原子力显微镜测量了其表面形貌和截面轮廓，结果如图 9 所示。所测聚苯胺线结构的表面均匀平滑，横截面高度与宽度一致，可将其截面形状近似为半椭圆形。线宽和高度如图 9(c)所示，所测横截面的高度为 323 nm，宽度为 392 nm，经计算可得 S 为 99444 nm^2。

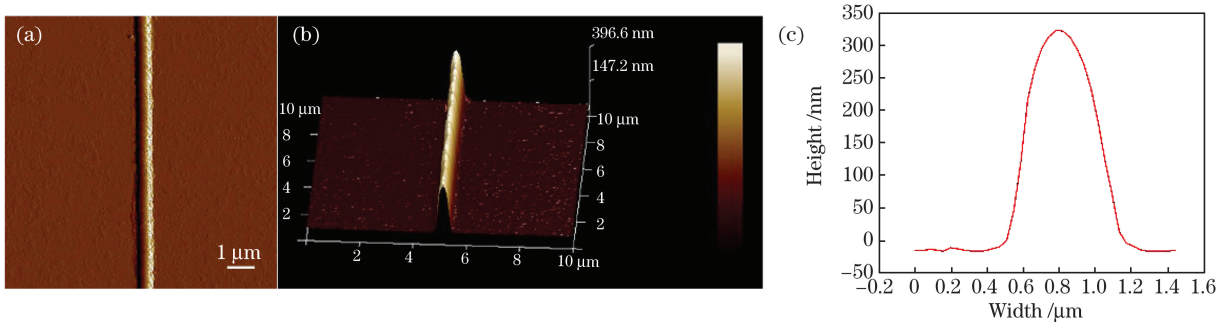

图 9　用于导电测试的聚苯胺线条的 AFM 图像及结果分析。(a)所测样品的 AFM 图；(b)所测样品截面的 3D 图；(c)所测样品的高度和线宽

Fig. 9　AFM image and result analysis of polyaniline line used for conductivity test. (a) AFM image of sample; (b) 3D AFM image of cross-section of sample; (c) height and width of sample

为测试聚苯胺微结构的导电性能，利用微操作低温探针台-半导体特征参数分析仪在氮气气氛下以−1.0～1.0 V 的扫描范围、0.05 V·s^{-1} 的扫描速度进行聚苯胺的电流-电压(C-V)曲线及其电阻值的测量，其原理示意图如图 10(a)所示。将两端镀有金电极的聚苯胺样品置于探针台的测试腔内，封闭测试腔并向其中注入氮气，然后操纵测试探针使其移动到纳米线两端的电极处，并确保接触良好，之后在相应的计算机界面完成聚苯胺纳米线的电阻测试。聚苯胺纳米线的 C-V 曲线如图 10(b)所示，测试电压范围为−1.0～1.0 V，电流随电压的增加呈现线性升高，这说明聚苯胺线具有导电性，线性拟合得到聚苯胺线的电阻 R 为 1.39×10^{12} Ω，通过进一步计算得到电导率 σ 为 5.79×10^{-6} S·cm^{-1}。

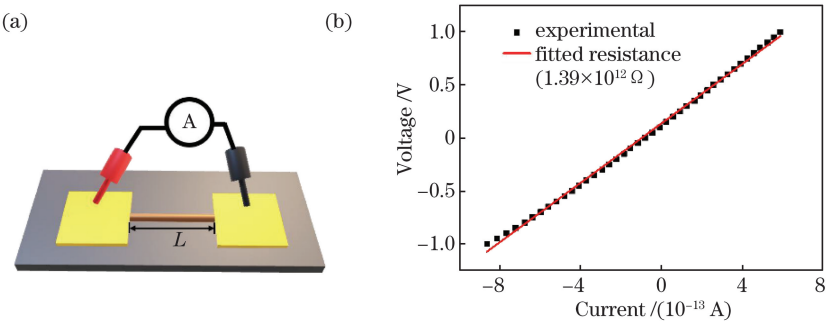

图 10　聚苯胺电阻测试。(a)测试原理图；(b)聚苯胺在 1.0 V 下的伏安曲线及其拟合电阻值

Fig. 10　Resistance test of polyaniline. (a) Diagram of test principle; (b) current-voltage curve measured at voltage of 1.0 V and fitted curve of resistance

4　结　　论

不同于传统的制备方法，基于飞秒激光双光子聚合的方法可在水相中直接制备导电聚合物聚苯胺，并且可实现对其微观形貌的精准可控。苯胺与硝酸的浓度是该方法的重要参量，在激光的作用下，两者的浓度及配比会影响苯胺低聚物的形成，当激光扫描路径上的苯胺单体基本形成苯胺低聚物时，制备的聚苯胺纳米线条的线型均匀，厚度较薄，而当激光扫描路径上的苯胺单体数量过多，苯胺低聚物

表现为三维高斯分布，在迁移距离的影响下形成具有凸包结构的聚苯胺线条。苯胺与硝酸的浓度比为 1.14∶1 时聚合性能最佳，在两者浓度分别为 0.69 mol·L^{-1}、0.60 mol·L^{-1}，激光功率为 14.1 mW，激光扫描速度为 6 μm·s^{-1} 的条件下，可制得结构连续、表面致密光滑且稳定性良好的聚苯胺纳米线。最后对该聚苯胺线进行了 FT-IR 测试和电导性测试，结果证明了聚苯胺的形成，通过计算得到其电导率为 5.79×10^{-6} S·cm^{-1}。本研究为导电聚合物微结构的可控制备提供了一种可行性方案，聚苯胺微纳米结构的可控制备可为导电聚合物在集成化器件中的应用提供新思路。

参 考 文 献

[1] Bhadra S, Khastgir D, Singha N K, et al. Progress in preparation, processing and applications of polyaniline[J]. Progress in Polymer Science, 2009, 34(8): 783-810.

[2] Wang Y M. Preparation and application of polyaniline nanofibers: an overview[J]. Polymer International, 2018, 67(6): 650-669.

[3] Tseng R J, Huang J, Ouyang J, et al. Polyaniline nanofiber/gold nanoparticle nonvolatile memory[J]. Nano Letters, 2005, 5(6): 1077-1080.

[4] Sun Z J, Zhang J M, Ye F, et al. Vulcanization treatment: an effective way to improve the electrochemical cycle stability of polyaniline in supercapacitors[J]. Journal of Power Sources, 2019, 443: 227246.

[5] Orachorn N, Bunkoed O. A nanocomposite fluorescent probe of polyaniline, graphene oxide and quantum dots incorporated into highly selective polymer for lomefloxacin detection[J]. Talanta, 2019, 203: 261-268.

[6] Ko Y, Jeong H Y, Kwon G, et al. pH-responsive polyaniline/polyethylene glycol composite arrays for colorimetric sensor application[J]. Sensors and Actuators B: Chemical, 2020, 305: 127447.

[7] Abd El-Lateef H M, Khalaf M M. Novel dispersed Tl_2O_3-SiO_2/polyaniline nanocomposites: *in-situ* polymerization, characterization and enforcement as a corrosion protective layer for carbon-steel in acidic chloride medium[J]. Colloids and Surfaces A: Physicochemical and Engineering Aspects, 2019, 573: 95-111.

[8] Han D H, Park S M. Electrochemistry of conductive polymers. 32. Nanoscopic examination of conductivities of polyaniline films[J]. The Journal of Physical Chemistry B, 2004, 108(37): 13921-13927.

[9] Yang C H, Huang L R, Chih Y K, et al. Molecular assembled self-doped polyaniline copolymer ultra-thin films[J]. Polymer, 2007, 48(11): 3237-3247.

[10] Kakaei K, Hamidi M, Kakaei N. Simultaneous electro-synthesis of polyaniline graphene nanocomposite in dilute graphene oxide as dopant and aniline by electrochemical method and its high specific capacitance[J]. Materials Research Express, 2019, 6(8): 085623.

[11] Liu B, Zhang X Y, Chen S Y, et al. Preparation and electrochemical energy storage performance of one dimensional orderly polyaniline nanowires array[J]. Chemical Journal of Chinese Universities, 2019, 40(3): 498-507.
刘奔, 张行颖, 陈韶云, 等. 一维有序聚苯胺纳米阵列的制备及电化学储能性能[J]. 高等学校化学学报, 2019, 40(3): 498-507.

[12] Xing J F, Zheng M L, Duan X M. Two-photon polymerization microfabrication of hydrogels: an advanced 3D printing technology for tissue engineering and drug delivery[J]. Chemical Society Reviews, 2015, 44(15): 5031-5039.

[13] Zheng M L, Jin F, Dong X Z, et al. Two-photon photopolymerization and functional micro/nanostructure fabrication[J]. Imaging Science and Photochemistry, 2017, 35(4): 413-428.
郑美玲, 金峰, 董贤子, 等. 双光子光聚合与功能微纳结构制备[J]. 影像科学与光化学, 2017, 35(4): 413-428.

[14] Shi Y, Xu B, Wu D, et al. Research progress on fabrication of functional microfluidic chips using femtosecond laser direct writing technology[J]. Chinese Journal of Lasers, 2019, 46(10): 1000001.
史杨, 许兵, 吴东, 等. 飞秒激光直写技术制备功能化微流控芯片研究进展[J]. 中国激光, 2019, 46(10): 1000001.

[15] Zhou X, Yang M, Zhang W, et al. Fiber hydrogen sensor coated with Pt-WO_3 film based on femtosecond laser micro-processing[J]. Chinese Journal of Lasers, 2019, 46(12): 1210001.
周贤, 杨沫, 张文, 等. 基于飞秒激光微加工的 Pt-WO_3 膜光纤氢气传感器[J]. 中国激光, 2019, 46(12): 1210001.

[16] Kawata S, Sun H B, Tanaka T, et al. Finer features for functional microdevices[J]. Nature, 2001, 412(6848): 697-698.

[17] Serbin J, Ovsianikov A, Chichkov B, et al. Fabrication of woodpile structures by two-photon polymerization and investigation of their optical properties[J]. Optics Express, 2004, 12(21): 5221-5228.

[18] Di J K, Zhou M, Yang H F, et al. Manufacturing micro-biological device and scaffold research with

two-photon femtosecond laser technology [J]. Chinese Journal of Lasers, 2009, 36(1): 249-254.
狄建科, 周明, 杨海峰, 等. 飞秒激光双光子制造生物微器件微支架[J]. 中国激光, 2009, 36(1): 249-254.

[19] Gou X R, Zheng M L, Zhao Y Y, et al. Mechanical property of PEG hydrogel and the 3D red blood cell microstructures fabricated by two-photon polymerization[J]. Applied Surface Science, 2017, 416: 273-280.

[20] Dong L, Agarwal A, Beebe D, et al. Variable-focus liquid microlenses and microlens arrays actuated by thermoresponsive hydrogels[J]. Advanced Materials, 2007, 19(3): 401-405.

[21] Sun R, Wang Z Y, Hu Y L, et al. Processing and application of hydrogel janus micropillars based on femtosecond laser [J]. Chinese Journal of Lasers, 2019, 46(9): 0902001.
孙锐, 王重宇, 胡衍雷, 等. 飞秒激光加工水凝胶双面神微柱及其应用[J]. 中国激光, 2019, 46(9): 0902001.

[22] Wang H, Lai T S, Lin W Z, et al. Femtosecond studies onthird-order optical nonlinearities of polyanilines [J]. Chinese Physics Letters, 1994, 11(8): 491-493.

[23] Li Z H, Lin W, Lu J T, et al. Reversed micelle synthesis of Ag/polyaniline nanocomposites via an *in situ* ultraviolet photo-redox mechanism[J]. Polymer Composites, 2012, 33(4): 451-458.

[24] Kim B J, Oh S G, Han M G, et al. Synthesis and characterization of polyaniline nanoparticles in SDS micellar solutions [J]. Synthetic Metals, 2001, 122(2): 297-304.

[25] Zhang Z M, Wei Z X, Wan M X. Nanostructures of polyaniline doped with inorganic acids[J]. Macromolecules, 2002, 35(15): 5937-5942.

[26] Wu X F, Yin H L, Li Q. Femtosecond laser processing of carbon nanotubes film [J]. Chinese Journal of Lasers, 2019, 46(9): 0902002.
吴雪峰, 尹海亮, 李强. 飞秒激光加工碳纳米管薄膜试验研究[J]. 中国激光, 2019, 46(9): 0902002.

[27] Du J, Li Y, Zhong Q, et al. Boosting the utilization and electrochemical performances of polyaniline by forming a binder-free nanoscale coaxially coated polyaniline/carbon nanotube/carbon fiber paper hierarchical 3D microstructure composite as a supercapacitor electrode[J]. ACS Omega, 2020, 5(35): 22119-22130.

[28] Stejskal J, Sapurina I, Trchová M, et al. Oxidation of aniline: polyaniline granules, nanotubes, and oligoaniline microspheres [J]. Macromolecules, 2008, 41(10): 3530-3536.

Fabrication of Polyaniline Microstructure via Two-Photon Polymerization

Wang Rongrong[1,3], Zhang Weicai[1,3], Jin Feng[1], Dong Xianzi[1], Liu Jie[1], Qu Liangti[2], Zheng Meiling[1*]

[1] *Key Laboratory of Bio-Inspired Materials and Interfacial Science, Technical Institute of Physics and Chemistry, Chinese Academy of Sciences, Beijing* 100190, *China*;

[2] *School of Machinery and Engineering, Tsinghua University, Beijing* 100084, *China*;

[3] *School of Future Technology, University of Chinese Academy of Sciences, Beijing* 101407, *China*

Abstract

Objective Polyaniline (PANI) has been intensively investigated owing to its low raw-material cost, high electrical conductivity, good environmental stability under ambient conditions, promising chemical, electrical, and optical properties, as well as its unusual doping characteristics. Therefore, PANI has been found to have a wide range of practical applications in many fields, such as supercapacitors, chemical/biological sensor devices, electromechanical actuators, anticorrosion coatings, separation membranes, and battery electrodes. The application basis of PANI is its synthesis. At present, PANI can be synthesized through various chemical/electrochemical approaches; however, the nanostructure uniformity of PANI at the large scale is poor, and the controlled growth of PANI microstructures is difficult in these preparation methods. Furthermore, it is unfavorable to realize the integration and miniaturization of devices. Hence, a synthetic method that is capable of developing regular, controllable, and uniform PANI nanostructures at a micro/nanoscale is required.

Two-photon polymerization (TPP) is a photopolymerization method based on the two-photon absorption effect and is an extremely powerful method to achieve real three-dimensional (3D) microdevices. Using femtosecond

lasers, which exhibit the characteristics of ultrashort pulse width, ultrahigh precision, and low heat input closely focused into a volume of polymer material, TPP has been employed in the fabrication of diverse micro-objects, such as biochips, micro/nanofluidic devices, and micro/nanoelectromechanical systems. Currently, two-photon polymeric materials are primarily commercial photoresists and hydrogels. These two-photon polymer materials can exhibit strong 3D processing capabilities and better biocompatibility; however, they do not exhibit electrical conductivity. Therefore, we attempt to propose the TPP method to prepare fine and controllable PANI structures and aim to provide new ideas for the preparation of conductive polymers and their wide applicability in sensors, microdetectors, and other micro/nano devices.

Methods PANI micro/nanostructures with diverse morphologies were fabricated using the TPP method based on femtosecond lasers. First, using aniline as the monomer and nitric acid as the oxidant, aniline mixed solutions with different molar ratios were prepared. Then, a drop of aniline mixed solution was fixed on the substrate, and the fabricated substrate was placed on the 3D moving stage for TPP processing. After that, a PANI microstructure attached to the glass substrate could be obtained. In addition, the morphology of the PANI microstructure was analyzed through scanning electron microscopy and atomic force microscopy, and the chemical composition of the PANI sample was characterized via Fourier transform infrared spectrometry (FT-IR). Current-voltage curves and resistance values of a single PANI line were tested using a micromanipulated cryogenic probe station-semiconductor characteristic parameter analyzer in a nitrogen atmosphere.

Results and Discussions PANI micro/nanowires with different morphologies can be prepared by adjusting the molar ratio of aniline to nitric acid (Fig. 3). The most prominent performance is whether the PANI lines are connected by convex hulls. Under the same laser power and scanning speed, when the molar ratio of aniline to nitric acid is relatively low (samples 1 and 4), it is easier to yield PANI lines with a relatively flat structure. As the concentration of the aniline monomer increased, the PANI lines became denser and thicker. Then, we illustrated the polymerization mechanism of aniline and explained the influence of the aniline concentration on the morphology of PANI lines (Fig. 4). The water-insoluble aniline polymer was synthesized at the water interface. The concentrations of aniline and nitric acid are closely related to the distribution of water-soluble aniline oligomers. When the concentration of aniline was low, the PANI lines with uniform and thin shapes were prepared because all of the aniline monomers in the laser scanning path at the laser focus were converted into aniline oligomers. When the number of aniline monomers in the laser scanning path was extremely large, PANI lines with a convex structure were prepared, which was attributed to the effect on the migration distance of the aniline oligomer with 3D Gaussian distributions. Although samples 1–4 can produce PANI lines, their performances are easily affected by the environment and the stability of the mobile station. To generate PANI with better conductivity and repeatability, we optimized the aniline mixed solution. The performance of the TPP of sample 5 was better than that of other samples (Fig. 5). In addition to the molar ratio of aniline to nitric acid, femtosecond laser power also affected the morphology of PANI lines. Under the high laser power, the PANI lines appear as a more discrete convex hull structure (Fig. 6). With the increasing laser scanning speed, the morphology of the PANI lines became looser, the intermittent situation was intensified, and the width of PANI lines reduced slightly (Fig. 7). Furthermore, FT-IR spectra of PANI were analyzed, which proved that PANI could be successfully prepared by TPP (Fig. 8). The electrical conductivities of the PANI lines were characterized and shown as 5.79×10^{-6} S·cm^{-1} (Fig. 10).

Conclusions To directly prepare microstructures of small-scale conductive polymers with controllable shape at one time, the TPP method based on femtosecond laser is proposed, which can realize the precise and controllable preparation of micro/nano-sized PANI. When the ratio of aniline to nitric acid was 1.14∶1, the concentration of aniline was 0.69 mol·L^{-1}, the laser power was 14.1 mW, and the laser scanning speed was 6 μm·s^{-1}. We could obtain the best performing of PANI lines with continuous structure, compact and smooth surface, and good stability. In addition, the FT-IR spectrum characterization of PANI lines demonstrates that PANI is successfully achieved using the TPP method. The electrical conductivity test of PANI shows that PANI is conductive, and its electrical conductivity is 5.79×10^{-6} S·cm^{-1}. This study provides a feasible solution for the controllable preparation of conductive polymer microstructures, and the controllable preparation of PANI micro/nanostructures can provide new ideas for the development of conductive polymers in integrated devices.

Key words laser optics; micro/nanostructure; two-photon polymerization; conductive polymer; polyaniline

OCIS codes 140.3390; 190.4180; 160.5470